Available online at www.sciencedirect.com
SCIENCE DIRECT
Journal of Catalysis 237 (2006) 29–37
JOURNAL OF CATALYSIS
www.elsevier.com/locate/jcat

Formaldehyde removal from air via a rotating adsorbent combined with a photocatalyst reactor: Kinetic modeling

Paul Chin, Lao P. Yang, David F. Ollis *

Department of Chemical and Biomolecular Engineering, Box 7905, North Carolina State University, Raleigh, NC 27695-7905, USA

Received 29 July 2005; revised 5 October 2005; accepted 8 October 2005

Available online 17 November 2005

Abstract

A novel rotating honeycomb adsorbent coupled with a photocatalytic reactor demonstrated by Shiraishi et al. is modeled here. In operation, the air pollutant formaldehyde was adsorbed from a simulated room (10 m^3) onto a slowly rotating honeycomb, which then passed slowly through a small chamber (0.09 m^3) in which locally recirculated heated air desorbed the formaldehyde and carried it through a photocatalytic reactor, which oxidized the desorbed material. The regenerated rotor-adsorbent then rotated back into the airtight chamber. This system was modeled at steady states and transient states to determine adsorption, desorption, and photocatalyst pseudo-first-order rate constants at the appropriate temperatures (ambient temperature for adsorption, 120–180 °C for desorption and photocatalysis). Intensity-corrected values for the photocatalytic rate constant k_{cat} ($cm^2/(mW\,s)$) deduced from fitting our model to the data of Shiraishi et al. were in good agreement with those calculated from five literature reports for formaldehyde photocatalytic destruction.

Keywords: Photocatalysis; Volatile organic compounds; Formaldehyde; Titanium dioxide; TiO_2; Adsorption; Desorption; Regeneration; Thermal swing; Kinetic model; Sick building syndrome

1. Introduction

The US Environmental Protection Agency (EPA) defines "sick building" syndrome (SBS) as a situation in which building occupants experience acute health conditions linked to time spent in a building, but no specific diagnosis can be assigned to their illness [1]. Often the occupants' symptoms disappear soon after they leave the building. Causes of SBS include inadequate ventilation, chemical contaminants from both indoor and outdoor sources, and biological contaminants. Volatile organic compounds (VOCs) are a category of indoor chemical contaminants, and formaldehyde (CH_2O) levels are of widespread interest. To prevent or eliminate SBS, building air must be cleaned or properly refreshed, and/or the sources of VOC pollutants removed or modified.

VOC is a diverse class of organic indoor air contaminants present in industrial (petroleum, pharmaceutical, textile), commercial (offices, restaurants), and residential buildings [2]. A VOC is defined by the U.S. EPA in the Code of Federal Regulations (CFR) [3] as any carbon compound (excluding certain compounds) participating in atmospheric photochemical reactions. Formaldehyde is one VOC that has been linked to SBS [4]. Formaldehyde is found in many indoor products, such as pressed wood, paints, insulation, coated paper products, and combustible materials. It is a colorless, strong-smelling gas that can cause nausea, chest tightness, wheezing, skin rashes, and allergic reactions at levels as low as 0.1 ppm [5]. It is a suspected human carcinogen and has been shown to cause cancer in animals. The Occupational Safety and Health Administration (OSHA) specifies a workplace time-weighted average permissible exposure limit (TWA-PEL) of 0.75 ppm, whereas the American Conference of Governmental Industrial Hygienists (ACGIH) recommends a TWA threshold limit value (TLV) of 0.3 ppm [6]. These time-weighted averages are for 8-h workdays or 40-h workweeks.

Techniques for VOC control in exhaust air streams include incineration, oxidation, wet scrubbing, ozonation, and adsorption [6,7]. Of these techniques, VOC adsorption on a solid

* Corresponding author. Fax: +1 919 515 3465.
E-mail addresses: paul.chin@ncsu.edu (P. Chin), ollis@eos.ncsu.edu (D.F. Ollis).

0021-9517/$ – see front matter
doi:10.1016/j.jcat.2005.10.013

surface holds the most promise for reducing SBS by treating ventilation air. The quantity of VOCs bound to the adsorbent depends on available adsorbent surface area, VOC concentration, temperature, VOC chemical structure, physical properties of adsorbent and VOC, adsorbent capacity or regenerated capacity, and contact time [7]. Two common adsorbents for indoor VOC removal are activated carbon and zeolites. Activated carbon is used predominantly to remove hydrocarbons and nonpolar gases, and zeolites are used predominately to remove polar gases and vapors [7]. Zeolites have been shown to remove benzene, *n*-hexane, and CH_2O from indoor air [8]. Activated carbon typically has a large surface area (1400 m^2/g) and modest density (0.55 g/cm^3). It is used to retain VOCs with molecular weights >45 and boiling points above 0 °C and is easily regenerated thermally [7]. Formaldehyde is a polar compound; its retentivity on activated carbon at 20 °C and 1 atm is ∼3% [9], where retentivity is defined as the maximum amount (wt%) of adsorbed vapor retained by the carbon after the ambient gas concentration reduces to zero.

The removal of VOCs from air using TiO_2 as a photocatalyst has been widely investigated. Peral and Ollis [10] degraded trace levels of gas-phase acetone, 1-butanol, CH_2O, and *m*-xylene on Degussa P25 TiO_2. Other studies have been conducted with CH_2O as a reactant [11–17]. Moreover, other VOCs (e.g., ethanol, acetaldehyde, methyl formate) are known to produce CH_2O as an intermediate species [18–22] during photocatalytic oxidation (PCO).

Ceramic honeycombs have been examined as catalyst supports for PCO. Honeycombs offer a number of advantages over pellet-shaped particles, including attrition resistance and low pressure drop even at high flow rates [2]. Suzuki [23] studied TiO_2 coated on cordierite monoliths for air purification in vehicles. Sauer and Ollis [22,24] coated anatase TiO_2 on ceramic monoliths and oxidized acetone, ethanol, and acetaldehyde in air. Son et al. [25] designed a combination of plasma with photocatalyst cordierite honeycomb substrate for removing propane, propene, toluene, *m*-xylene, ammonia, trimethylamine, and methylmercaptane.

Honeycomb monoliths have also been used as supports for thermally regenerable adsorbents. In one configuration, a rotating honeycomb adsorbent is used to cycle through process (adsorption) and regeneration (desorption) zones to remove contaminants. In the adsorption or process zone, organic impurities are removed from the inflowing stream by adsorption on the rotor. In the subsequent high-temperature regeneration zone, these impurities desorb from the rotor into a second, isolated air flow. Some rotor sorbent configurations include a cooling zone to rapidly decrease the honeycomb temperature just after the regeneration zone. Researchers have studied rotating zeolite-coated honeycombs for VOC removal [26,27]. For removing acetone, isopropyl alcohol, propylene glycol monomethyl ether acetate, and propylene glycol methyl ether from air, Chang et al. [26] found an optimal rotation speed of 3–4.5 rotations/h for a process temperature of 40 °C and a regeneration temperature of 180 °C. Mitsuma et al. [27] developed an optimal empirical formula for rotation speed for cyclohexanone adsorption on a ceramic honeycomb rotor impregnated with a high-silica zeolite. For 30 and 200 ppm cyclohexanone concentrations, the optimal rotation speed was a function of the desorption gas stream velocity, the rotor width, and the ratio of the monolith cross-sectional area in the process zone to the monolith area in the desorption zone. Typical values ranged from 20 to 50 rotations/h.

Combination PCO reactor–adsorbent systems also have been examined. Ao and Lee [28] studied toluene and nitrogen oxide removal using TiO_2 immobilized on an activated carbon filter. Combining adsorption, thermal regeneration and photocatalysis, Shiraishi et al. [29] developed a novel air-purification system consisting of a rotating honeycomb loaded with zeolite or activated carbon, combined with a TiO_2 reactor to remove and eventually photocatalytically oxidize the air contaminant CH_2O. In a batch system (airtight chamber) with initial CH_2O levels of 0.55–0.75 mg/m^3, this system achieved the 0.1 mg/m^3 CH_2O guideline set by the World Health Organization in 10 min and reached nearly zero concentration after 90 min. Our work constructs an engineering model for their combined adsorbent–PCO reactor system.

Except for CH_2O source removal in indoor products, the technology developed by Shiraishi et al. [29] is believed to be the best option for removing existing levels of CH_2O. Their system decreases the CH_2O concentration in a simulated room below the WHO guideline, in addition to oxidizing the CH_2O in a small PCO reactor. Adsorption-only systems to a sorbent material require frequent sorbent replacement or regeneration. Increased fresh air ventilation and removal of exhaust air require increased energy consumption, because air is not recirculated. Energy is expended to cool or heat the fresh air to the desired temperature, and the CH_2O-containing air is exhausted outdoors, polluting the atmosphere. Ozonation can be used to oxidize CH_2O, but ozone can damage the respiratory system.

We report the development of a kinetic model for a novel rotating adsorbent–photocatalyst reactor. The combination adsorbent–catalyst system allows rapid air contaminant removal (air to adsorbent), followed by desorption into a small-volume photoreactor, where the consequent three- to five-fold increase in contaminant concentration allows the use of a smaller reactor than a photocatalyst-only system would require.

2. Experimental

2.1. Experimental apparatus

The process modeled includes two independent, continuous-flow systems interconnected by a rotating, cylindrical ceramic honeycomb. The rotation cycles the honeycomb rotor through a low-temperature process (adsorption) and a high-temperature regeneration (desorption) zone to remove CH_2O from chamber air. A diagram of the experimental system is reproduced in Fig. 1 [29]. In greater detail, the system comprises of an airtight chamber ("highly tight room" in the Shiraishi article), a cylindrical honeycomb ceramic rotor, a small box chamber, and a photocatalytic reactor contained therein. The volumes of the airtight chamber (simulated room) and small box are 10

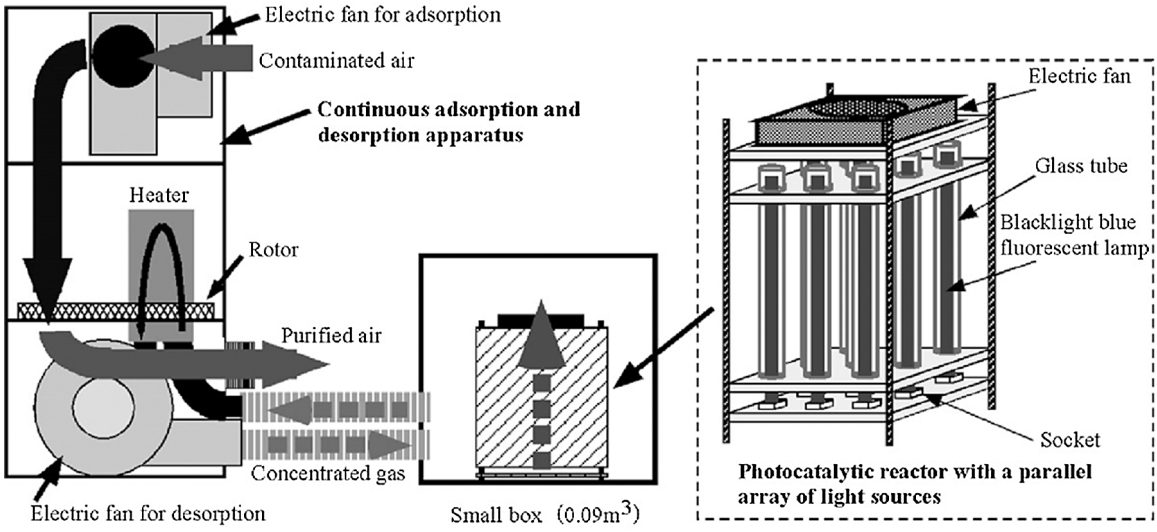

Fig. 1. A schematic of an air-purification system consisting of the photocatalytic reactor with a parallel array of nine blacklight-blue fluorescent lamps and the continuous adsorption and desorption apparatus with a ceramic-paper honeycomb rotor retaining activated carbon or zeolite fine particles (reproduced from Shiraishi et al. [29]).

and 0.09 m^3, respectively. The rotating honeycomb passes alternately through the airtight chamber and the small box chamber containing the PCO reactor (∼0.014 m^3). The combination system provides a greater than four-fold increase in initial CH_2O concentration than the airtight chamber. The higher CH_2O concentration in the small box reduces the required size of the PCO reactor accordingly.

The rotor (300 mm diameter, 50 mm thick) is composed of ceramic honeycomb laminates with a 3-mm corrugation pitch. Shiraishi et al. [29] deposited a zeolite (ZSM-5) or activated carbon (coconut husk) on the rotor to adsorb CH_2O. Because they found that activated carbon is a better adsorbent for CH_2O, our model examines only their data for this system. The rotation speed of their honeycomb is not specified, but it is assumed to be slow enough so that the higher temperature in the small box does not elevate the temperature in the airtight chamber.

The photocatalytic reactor consists of nine 6-W blacklight-blue fluorescent lamps enclosed in Pyrex glass tubes. The lamps emit primarily in the UVA (300–400 nm) wavelengths. The Pyrex tubes are 230 mm long and have a 28 mm i.d. A thin TiO_2 film is deposited on the inside surface of the glass tubes, concentric to the lamps. The total superficial photocatalyst surface area is 0.182 m^2. The distance from the lamp surface to the TiO_2 photocatalyst film is 3.5 mm. The lamp intensity at the TiO_2 surface is estimated by our calculations as 9 mW/cm^2.

At the start of a batch adsorption–desorption experiment [29], an initial dose of CH_2O was added to the airtight chamber. Independent air streams recirculated within the 10 m^3 chamber and the 0.09 m^3 small box, with no fresh air added at any time. In the simple adsorption–desorption experiments, CH_2O is transferred from the airtight chamber to the small box via adsorption to and desorption from the rotor until steady state is reached. In the batch adsorption–desorption with reaction experiments, the PCO reactor is placed in the small box and operated concurrently with the rotating honeycomb.

2.2. Model and parameter estimation

The following sections discuss the model development and parameter evaluation method.

2.2.1. Adsorption–desorption equilibrium constants

Data from the simple adsorption–desorption experiments from Shiraishi et al. [29] are used to calculate the adsorption equilibrium constants $K_{\text{AC-CHR}}$ and $K_{\text{SB-CHR}}$ at ambient and desorption/regeneration temperatures, respectively. The total quantity of CH_2O in the system is constant, because no reaction occurs in these experiments. A CH_2O mole balance is used to calculate the amount of CH_2O adsorbed on the honeycomb rotor:

$$\begin{aligned}(\text{initial amount}) &= (\text{airtight chamber}) + (\text{small box})\\ &\quad + (\text{ceramic honeycomb rotor}),\end{aligned}$$

$$V_{\text{AC}}C_0 = V_{\text{AC}}C_{\text{AC}} + V_{\text{SB}}C_{\text{SB}} + V_{\text{CHR}}C_{\text{CHR}}. \tag{1}$$

The experimental conditions state that 5/6 of the rotor resides in the airtight chamber, with only 1/6 located in the small box. This separation is used to split the amount of CH_2O on the rotor. This is an approximation, because the adsorption and desorption temperatures are different. More CH_2O desorbs from the rotor at higher temperatures. Therefore, the amount of CH_2O on the hot rotor in the small box is smaller than we estimate:

$$\begin{aligned}&\text{mol of } CH_2O \text{ on the cold rotor in airtight chamber}\\ &\quad = \left(\frac{5}{6}V_{\text{CHR}}\right)C_{\text{CHR}},\\ &\text{mol of } CH_2O \text{ on the hot rotor in small box}\\ &\quad = \left(\frac{1}{6}V_{\text{CHR}}\right)C_{\text{CHR}}.\end{aligned} \tag{2}$$

A simple rate expression is developed for CH_2O adsorption on and desorption from the rotor. For the low CH_2O levels of interest (<3 mg/m^3 or <2.4 ppm), we assume that both adsorption and desorption are first order in CH_2O on a sparsely covered surface:

Adsorption side:

$$\mathrm{CH_2O_{airtight\ chamber\ (gas)}} \underset{k_{\mathrm{des}}(T_{\mathrm{ads}})}{\overset{k_{\mathrm{ads}}(T_{\mathrm{ads}})}{\rightleftharpoons}} \mathrm{CH_2O_{rotor\ (ads)}},$$

$$\begin{aligned} -V_{\mathrm{AC}}\frac{\mathrm{d}C_{\mathrm{AC}}}{\mathrm{d}t} &= \frac{5}{6}V_{\mathrm{CHR}}\frac{\mathrm{d}C_{\mathrm{CHR}}}{\mathrm{d}t} \\ &= V_{\mathrm{AC}}k_{\mathrm{ads}}(T_{\mathrm{ads}})C_{\mathrm{AC}} - \frac{5}{6}V_{\mathrm{CHR}}k_{\mathrm{des}}(T_{\mathrm{ads}})C_{\mathrm{CHR}}. \end{aligned} \tag{3}$$

Desorption side:

$$\mathrm{CH_2O_{rotor\ (ads)}} \underset{k_{\mathrm{ads}}(T_{\mathrm{des}})}{\overset{k_{\mathrm{des}}(T_{\mathrm{des}})}{\rightleftharpoons}} \mathrm{CH_2O_{small\ box\ (gas)}},$$

$$\begin{aligned} V_{\mathrm{SB}}\frac{\mathrm{d}C_{\mathrm{SB}}}{\mathrm{d}t} &= -\frac{1}{6}V_{\mathrm{CHR}}\frac{\mathrm{d}C_{\mathrm{CHR}}}{\mathrm{d}t} \\ &= \frac{1}{6}V_{\mathrm{CHR}}k_{\mathrm{des}}(T_{\mathrm{des}})C_{\mathrm{CHR}} - V_{\mathrm{SB}}k_{\mathrm{ads}}(T_{\mathrm{des}})C_{\mathrm{SB}}. \end{aligned} \tag{4}$$

For adsorption–desorption-only experiments, a steady state is predicted, at which time the net change in concentrations is 0. In this case (3) and (4) are equal to 0, and the adsorption equilibrium constants (i.e., ratio of rate constants) are solved from the system's steady-state data. In the adsorption–desorption-only experiments, Shiraishi et al. [29] stated that the CH_2O concentration in both rooms remained relatively unchanged after 900 s (15 min). A system steady state, corresponding approximately to an adsorption–desorption equilibrium between the chamber, rotor, and box, had been achieved. Thus we solve for $K_{\text{AC-CHR}}$ and $K_{\text{SB-CHR}}$ using the data after 900 s. The K values are averaged using the data points from 1800–7200 s (30–120 min). The small decrease in CH_2O concentration at longer time (10,800 s) is neglected:

$$K_{\text{AC-CHR}}(T_{\mathrm{ads}}) = \frac{k_{\mathrm{ads}}(T_{\mathrm{ads}})}{k_{\mathrm{des}}(T_{\mathrm{ads}})} = \frac{(5/6)V_{\mathrm{CHR}}C_{\mathrm{CHR}}}{V_{\mathrm{AC}}C_{\mathrm{AC}}} \tag{5}$$

and

$$K_{\text{SB-CHR}}(T_{\mathrm{des}}) = \frac{k_{\mathrm{ads}}(T_{\mathrm{des}})}{k_{\mathrm{des}}(T_{\mathrm{des}})} = \frac{(1/6)V_{\mathrm{CHR}}C_{\mathrm{CHR}}}{V_{\mathrm{SB}}C_{\mathrm{SB}}}. \tag{6}$$

The adsorption equilibrium constant is dependent on temperature. Hence we find only one $K_{\text{AC-CHR}}$ constant (T_{ads} = ambient) of 3.28, but three $K_{\text{SB-CHR}}$ constants (T_{des} = 120, 150, and 180 °C) of 4.76, 4.07, and 2.70, respectively.

2.2.2. Adsorption rate constant in the airtight chamber

Given $K_{\text{AC-CHR}}$, Eq. (3) can be rearranged in terms of $K_{\text{AC-CHR}}$ instead of $k_{\mathrm{des}}(T_{\mathrm{ads}})$. This allows us to solve for $k_{\mathrm{ads}}(T_{\mathrm{ads}})$, because $K_{\text{AC-CHR}}$ is calculated from the method described above. The derivative term is obtained by the Differentiate function in Microcal Origin. All adsorption experiments were conducted at one temperature (T_{ads}), presumably ambient:

$$-V_{\mathrm{AC}}\frac{\mathrm{d}C_{\mathrm{AC}}}{\mathrm{d}t} = k_{\mathrm{ads}}(T_{\mathrm{ads}})\left\{V_{\mathrm{AC}}C_{\mathrm{AC}} - \frac{(5/6)V_{\mathrm{CHR}}C_{\mathrm{CHR}}}{K_{\text{AC-CHR}}(T_{\mathrm{ads}})}\right\}. \tag{7}$$

2.2.3. Desorption rate constants in the small box

The desorption rate constant, $k_{\mathrm{des}}(T_{\mathrm{des}})$, is fitted to the data of Shiraishi et al. An Arrhenius form is assumed for k_{des}. With $k_{\mathrm{des},0}$ taken as 10^{13} s^{-1}, the $E_{\mathrm{A,des}}$ fitted to the data is 107 kJ/mol (25.6 kcal/mol). The pre-exponential factor for desorption is the same order of magnitude as reported in the literature for first-order desorption kinetics [30,31]. The fitted activation energy of desorption is a typical value for weakly chemisorbed molecules on TiO_2. Lewandowski and Ollis [30] used the TPO/TPD data of Larson and Falconer [32] to estimate an $E_{\mathrm{A,des}}$ of 23–28 kcal/mol for benzene, toluene, and xylene. Chemisorbed molecules characteristically have desorption activation energies >50–100 kJ/mol (12–24 kcal/mol) [33]. Aldehydes are known to chemisorb weakly on TiO_2 (vs. alcohols or carboxylic acids), hence their common appearance as reaction intermediates [22,32]. Our fitted $E_{\mathrm{A,des}}$ falls within or just above these estimations. With these $k_{\mathrm{des},0}$ and $E_{\mathrm{A,des}}$ values, three k_{des} are calculated, one for each desorption temperature (i.e., 120, 150, and 180 °C):

$$k_{\mathrm{des}}(T_{\mathrm{des}}) = k_{\mathrm{des},0}\exp\left(\frac{-E_{\mathrm{A,des}}}{RT_{\mathrm{des}}}\right). \tag{8}$$

2.2.4. Reaction rate constant

Our photocatalytic rate constant, $k_{\mathrm{cat}}(T_{\mathrm{des}})$, was also fitted to the data of Shiraishi et al. [29] from the combined, simultaneous operation of the rotating honeycomb and PCO reactor. A pseudo-first-order reaction rate is assumed for CH_2O destruction. Obee and Brown [11] reported a first-order CH_2O oxidation rate at ambient temperatures for CH_2O concentrations pertinent to problematic buildings, which include the conditions of Shiraishi et al. [29] (~0.5–2.0 ppmv). At a 180 °C (453 K) desorption temperature, the best fit for k_{cat} is 2.38×10^{-2} s^{-1}. At 120 °C (393 K) and 150 °C (423 K), the best fits for k_{cat} are 1.19×10^{-1} and 1.06×10^{-1} s^{-1}, respectively.

The negative influence of temperature on apparent rate constant is rationalized as follows: A catalyzed reaction following a Langmuir–Hinshelwood rate form (as do most air contaminants including CH_2O) will provide a reaction rate form at low concentrations of

$$\begin{aligned} r_{\mathrm{cat}} &= -k_{\mathrm{cat}}C_{\mathrm{SB}}V_{\mathrm{rxr}} = -k_{\mathrm{rxn}}K_{\mathrm{ads}}C_{\mathrm{SB}}V_{\mathrm{rxr}} \\ &= -k_{\mathrm{rxn}}\left[\frac{k_{\mathrm{ads,TiO_2,0}}\exp(-E_{\mathrm{ads,TiO_2}}/(RT_{\mathrm{ads}}))}{k_{\mathrm{des,TiO_2,0}}\exp(-E_{\mathrm{des,TiO_2}}/(RT_{\mathrm{des}}))}\right]C_{\mathrm{SB}}V_{\mathrm{rxr}}, \end{aligned} \tag{9}$$

$$\begin{aligned} r_{\mathrm{cat}} &= -k_{\mathrm{rxn}}\frac{k_{\mathrm{ads,TiO_2,0}}}{k_{\mathrm{des,TiO_2,0}}} \\ &\quad\times\exp\left[\frac{1}{R}\left(\frac{E_{\mathrm{des,TiO_2}}}{T_{\mathrm{des}}} - \frac{E_{\mathrm{ads,TiO_2}}}{T_{\mathrm{ads}}}\right)\right]C_{\mathrm{SB}}V_{\mathrm{rxr}} \\ &\approx -k_{\mathrm{rxn}}\frac{k_{\mathrm{ads,TiO_2,0}}}{k_{\mathrm{des,TiO_2,0}}}\exp\left(\frac{E_{\mathrm{app}}}{RT_{\mathrm{des}}}\right)C_{\mathrm{SB}}V_{\mathrm{rxr}}. \end{aligned}$$

Thus,

$$k_{\mathrm{cat}} \approx k_{\mathrm{rxn}}\frac{k_{\mathrm{ads,TiO_2,0}}}{k_{\mathrm{des,TiO_2,0}}}\exp\left(\frac{E_{\mathrm{app}}}{RT_{\mathrm{des}}}\right) \quad \text{and}$$

$$\Delta H_{\mathrm{ads,TiO_2}} \approx E_{\mathrm{des,TiO_2}}.$$

Table 1
A comparison of our pseudo-first-order reaction rates (k_{cat}) and formal quantum efficiencies (δ) to literature data

	UV flux (mW/cm^2)	Reaction temp. (°C)	k_{cat} (s^{-1})	Normalized k_{cat} ($cm^2/(mW\,s)$)	FQE[a]	Catalyst manufacturer	Reference
This article	9	120–180	2.38×10^{-2} to 1.19×10^{-1}	2.6×10^{-3} to 1.3×10^{-2}	6×10^{-4} to 2×10^{-3} (~2 ppm)	–	–
Obee and Brown[b,c]	9.3	~22–24	2.2×10^{-3}	2.4×10^{-4}	1.5×10^{-2} (~1.2 ppm)	Degussa P25	[11]
Obee[b]	0.33	~22	5.8×10^{-4}	1.8×10^{-3}	1.2×10^{-1} (~1.2 ppm)	Degussa P25	[12]
Noguchi et al.[b]	1	~22	2.1×10^{-3}	2.1×10^{-3}	6×10^{-2} (~3 ppm)	Ishihara Sangyo	[15]
Ching et al.	0.6 (solar) 1.56 (UV)	Room temp.	1.5×10^{-3} 2.6×10^{-3}	2.4×10^{-3} 1.8×10^{-3}	2×10^{-3} (~100 ppm)	Self prepared & Degussa P25	[16]
Ao et al.[b]	0.75	Room temp.	6.8×10^{-4}	9.1×10^{-4}	–	Degussa P25	[17]

[a] Formal quantum efficiencies were estimated from literature data.
[b] Pseudo-first-order k_{cat} values were estimated from literature data.
[c] Obee and Brown ran experiments at multiple temperatures, but only the room temperature data is reported here

(We assume that the k_{rxn} of a free radical (e.g., OH·) is approximately independent of temperature. Using the fitted k_{cat} values variation with temperature.) We estimate the apparent activation energy of CH_2O desorption on TiO_2 (E_{app}) as 39 kJ/mol (9.3 kcal/mol). We expect a small (or zero) value for E_{ads,TiO_2} (e.g., CH_2O may need to displace weakly bound water) and a substantial value for E_{des,TiO_2} (e.g., 20–30 kcal/mol). We expect the term $(E_{des,TiO_2}/T_{des} - E_{ads,TiO_2}/T_{ads}) > 0$, and thus expect that k_{cat} will decrease with increasing temperature, reflecting decreased CH_2O coverage on the TiO_2 with increasing temperature. A summary of our k_{cat} values and those in the literature is given in Table 1. Authors of the literature reported herein used various reactor geometries, so we chose a reactor volume basis (V_{rxr}) to simplify calculations.

Table 1 compares the reaction rate constants evaluated in this study with those in the literature. Reaction rates are dependent on the catalyst manufacturer and on the UV light intensity, among other factors. We derived pseudo-first-order kinetic rate constants from CH_2O data for PCO collected by other researchers, using CH_2O concentrations similar to those of Shiraishi et al. (~2 ppm at STP). Data from Obee [12] and Obee and Brown [11] were used to derive a first-order k_{cat} of 5.8×10^{-4} and 2.2×10^{-3} s^{-1}, respectively, for UV light intensities ranging from 0.33 to 9.3 mW/cm^2. Data from Noguchi et al. [15] and Ao et al. [17] were also used to calculate a k_{cat} of 2.1×10^{-3} and 6.8×10^{-4} s^{-1}, respectively, for UV light intensities between 0.75 and 1.0 mW/cm^2. Ching et al. [16] found first-order k_{cat} values of 1.5×10^{-3} and 2.6×10^{-3} s^{-1} using solar and UV light intensities of 0.6 and 1.56 mW/cm^2, respectively. The k_{cat} in our study ranges from 2.38×10^{-2} to 1.19×10^{-1} s^{-1}. Shiraishi et al. [29] reported a UV light intensity of 15 $\mu W/cm^2$, which is low for nine 6-W blacklight-blue fluorescent lamps. Instead, our calculations estimate an intensity of 9 mW/cm^2 for their data, assuming 30% blacklight-blue emission efficiency. The brand of TiO_2 catalyst used in the study of Shiraishi et al. is not listed. The two brands used by other authors discussed above are Degussa P25 or Ishihara Sangyo. Our calculated k_{cat} values fall in the high end and above the range derived from the work of these authors.

The k_{cat} derived from various authors' data are normalized by their UV light intensity to account for this variation. Ching et al. [16] and Sauer and Ollis [22] report that at low UV intensities, the reaction rate is proportional to the irradiance (I), and that at medium to higher UV intensities, the reaction rate is often proportional to I^n, where $0.5 < n < 1$. If all of the reported irradiances for CH_2O PCO are low intensity, we may divide k_{cat} by their irradiances (mW/cm^2). The normalized k_{cat} for the authors discussed above range from 2.4×10^{-4} to 2.5×10^{-3} $cm^2/(mW\,s)$ at ambient temperature (Table 1). The normalized k_{cat} values in our study range from 2.6×10^{-3} to 1.3×10^{-2} $cm^2/(mW\,s)$. Again, our values are in the high end and above the range derived from other authors' data. We note that other reports pertain to ambient temperature photocatalysis, versus Shiraishi et al. [29] for which T(reaction) ~ T(desorption: 120–180 °C).

At high UV intensities, photodissociation (photolysis) of CH_2O can occur and potentially complicate interpretation of PCO data for CH_2O. The fitted k_{cat} in our study is a bulk term that includes both photocatalytic and any photolytic effects. Obee and Brown [11] explored this issue, finding a linear relationship between UV flux and CO evolution from CH_2O photolysis. At 7 mW/cm^2, they observed no CO evolution in a stream with initial 3.3 ppmv CH_2O. At 25 mW/cm^2, they observed 0.10 ppmv CO evolution. Assuming a linear relationship, the data from Shiraishi et al. [29] would produce 0.03 ppmv CO from photolysis at 9 mW/cm^2. Thus, less than 1.5% of the CH_2O would photodissociate, using a 1:1 CH_2O:CO relationship. This 1:1 ratio is similar to the data reported by Obee and Brown [11] and predicted by Okabe [34]. Moreover, Ching et al. [16] found the photolytic rate constant to be ~10 times smaller than the photocatalytic rate constant at a solar irradiance of 0.6 mW/cm^2. Hence we believe the photolytic contribution to CH_2O disappearance is negligible in the data of Shiraishi et al. and thus do not include it in our model.

Table 2
Summary of the parameters calculated or fitted in the model

Temperature (°C)	$k_{ads}(T_{ads})$ (s^{-1})	$k_{des,0}$ (s^{-1})	$E_{A,des}$ (kJ/mol)	$k_{des}(T_{des})$ (s^{-1})	$K_{AC\text{-}CHR}$	$K_{SB\text{-}CHR}$	$k_{cat}(T_{des})$ (s^{-1})
T_{ads}	4.33×10^{-4}	–	–	–	3.28	–	–
120 °C	–	10^{13}	107	0.0607	–	4.76	0.119
150 °C	–	10^{13}	107	0.618	–	4.07	0.106
180 °C	–	10^{13}	107	4.63	–	2.70	0.0238

2.3. Overall models

After all of the parameters are calculated or fitted, two equations for each model result, one equation for the airtight chamber and one for the small box. Equation (7) is used for CH_2O adsorption on the rotor from the airtight chamber. In the adsorption–desorption-only model, Eq. (4) is rearranged to estimate CH_2O desorption from the rotor to the small box (Eq. (10)). In the desorption/reaction model, Eq. (11) includes the PCO reaction in the small box. Table 2 summarizes all of the calculated and fitted parameters in the two models.

Without reaction:

$$V_{SB}\frac{dC_{SB}}{dt} = k_{des}(T_{des}) \times \left(\frac{1}{6}V_{CHR}C_{CHR} - K_{SB\text{-}CHR}(T_{des})V_{SB}C_{SB}\right). \quad (10)$$

With reaction:

$$V_{SB}\frac{dC_{SB}}{dt} = k_{des}(T_{des}) \times \left(\frac{1}{6}V_{CHR}C_{CHR} - K_{SB\text{-}CHR}(T_{des})V_{SB}C_{SB}\right) - k_{cat}(T_{des})V_{rxr}C_{SB}. \quad (11)$$

3. Calculated results and discussion

3.1. Adsorption–desorption-only model

Fig. 2 shows the model and data of Shiraishi et al. in both rooms at a desorption temperature of 180 °C. In the airtight chamber, the adsorption model fits the data well, accurately predicting the initial $C_{AC}(t)$ profile (0–1800 s). At longer times, the adsorption equilibrium value C_{AC}(equil) is smaller than predicted. In the small box, the desorption model provides a reasonable fit to the data. The model predicts the initial $C_{SB}(t)$ profile (0–300 s) well. The monotonic decrease in this data under dark conditions between 3600 and 10,800 s may be caused by an effect that is not considered; for example, slow dimerization of CH_2O to paraformaldehyde may occur on the adsorbent. Similar data for the model and the data of Shiraishi et al. at 120 and 150 °C desorption temperatures are shown in Fig. 3. At all desorption temperatures, the residual error between our model and the data of Shiraishi et al. falls within ±0.07 mg/m^3 in the airtight chamber and within ±0.3 mg/m^3 in the small box with the exception of two data points.

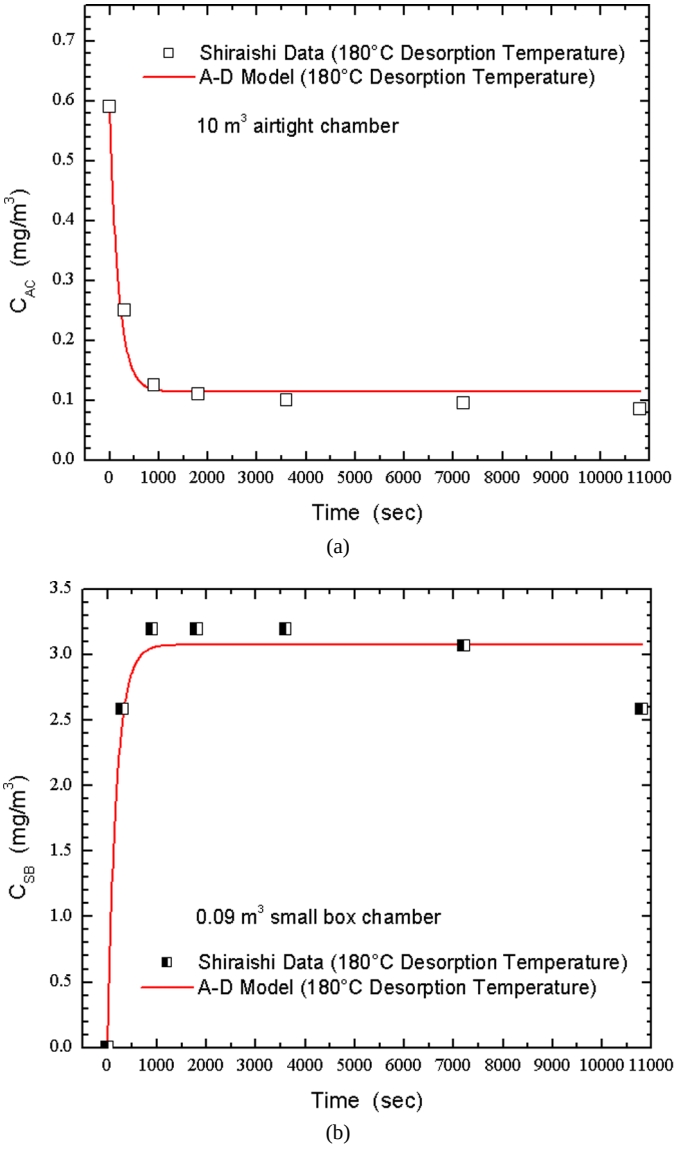

Fig. 2. Shiraishi data and model of adsorption–desorption-only at 180 °C desorption temperature in (a) the airtight chamber and (b) the small box.

3.2. Adsorption–desorption and reaction model

The model described above is modified to include the PCO reactor in the small box. Fig. 4 shows the model and the data of Shiraishi et al. in both rooms at a desorption temperature of 180 °C. In the airtight chamber, the adsorption model follows the trend of the data. At 10,800 s (180 min), both the data and the model approach zero for C_{AC}, as expected be-

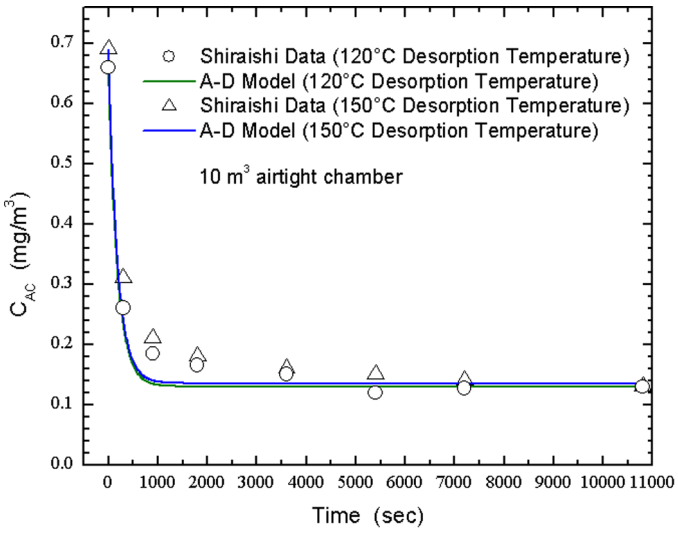

(a)

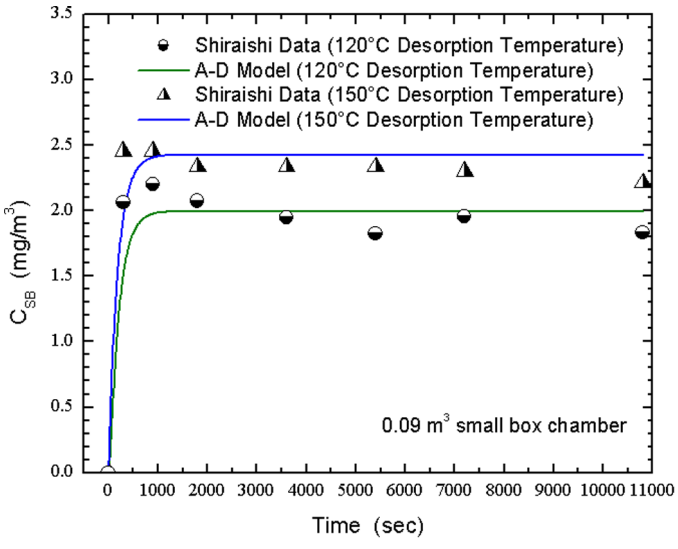

(b)

Fig. 3. Shiraishi data and model of adsorption–desorption-only at 120 and 150 °C desorption temperatures in (a) the airtight chamber and (b) the small box.

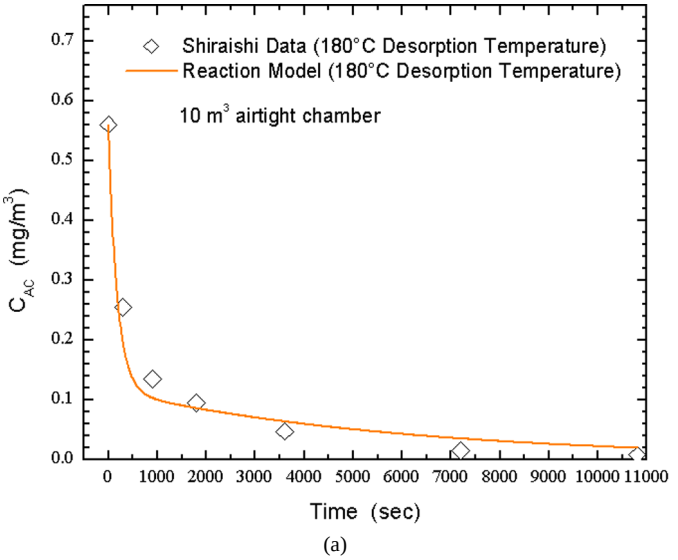

(a)

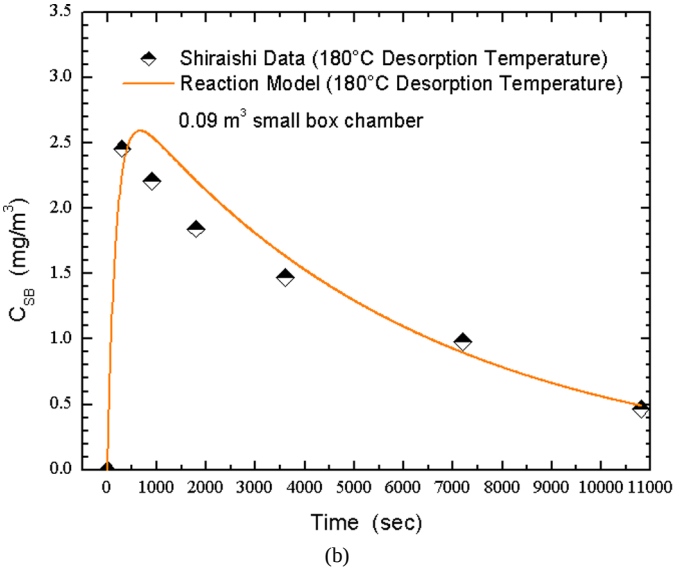

(b)

Fig. 4. Shiraishi data and model of adsorption–desorption with photocatalytic reaction at 180 °C desorption temperature in (a) the airtight chamber and (b) the small box.

cause CH_2O is continuously oxidized photocatalytically in the small box. In the small box, the reaction model also provides a reasonable fit to the desorption and reaction data. The model qualitatively describes the increase and subsequent decrease in C_{SB} caused by the reaction. Results for the model and the data of Shiraishi et al. at desorption temperatures of 120 and 150 °C are shown in Fig. 5. At all desorption temperatures, the residual error falls within ± 0.05 mg/m^3 in the airtight chamber and within ± 0.3 mg/m^3 in the small box.

The fitted values of k_{cat} for the 120 and 150 °C desorption temperatures are almost an order of magnitude larger than the 180 °C value. Shiraishi et al. [29] attributed a marked loss in photocatalytic activity (and a consequent decrease in k_{cat}) at 180 °C to unknown substances liberated from the activated carbon rotor and strongly adsorbed on the glass surface of the TiO_2 reactor. Such film formation would decrease the intensity of light arriving at the photocatalyst surface; hence the resultant decrease in k_{cat}. An alternative explanation is that the k_{cat} used here is a bulk term that includes both CH_2O adsorption on TiO_2 and the true reaction rate constant, as described above. Adsorption decreases with increasing temperature, lowering CH_2O coverage. There are similar orders of magnitude decreases in k_{cat} and K_{SB} with increasing temperature, consistent with the idea that k_{cat} is dominated by the temperature dependence of adsorption.

The quantum yield ($\Phi_{overall}$) is defined as the rate of photoreaction divided by the rate of light absorption [35]. The latter is difficult to estimate using the data of Shiraishi et al. Incident light from the lamp may be absorbed, reflected, or scattered upon reaching the catalyst surface. Instead, a formal quantum efficiency (FQE) of the system is calculated, defined as [35,36]

$$\delta = \frac{\text{rate of photocatalyzed reaction (molecules/s)}}{\text{incident light intensity (photons/s)}}. \qquad (12)$$

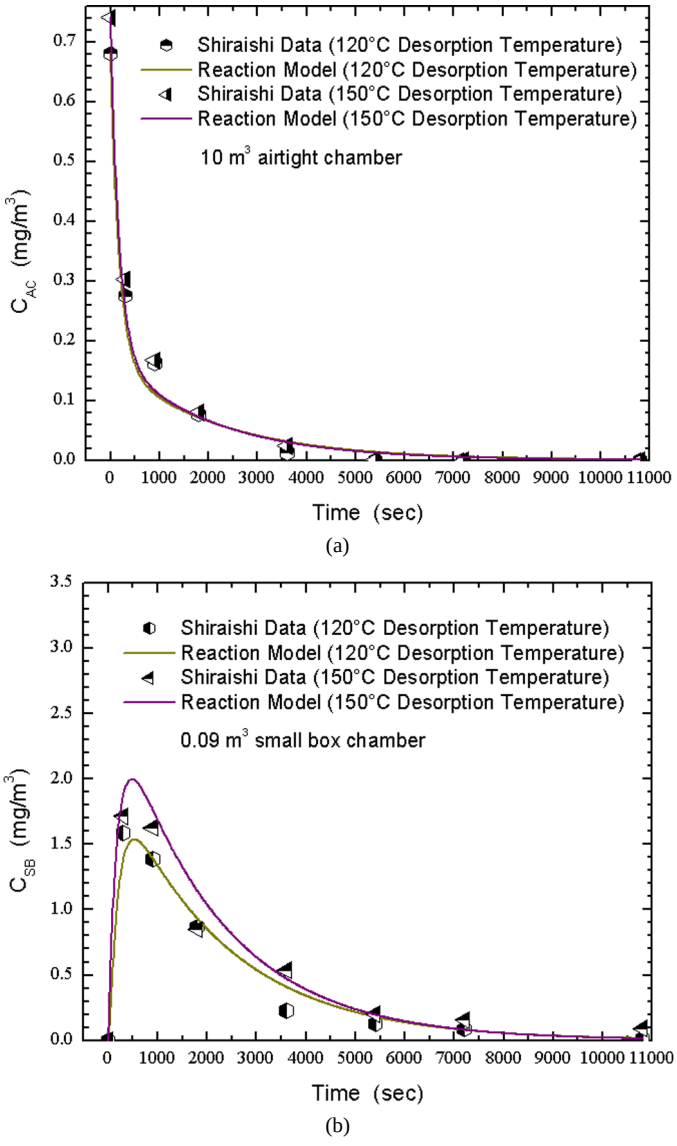

Fig. 5. Shiraishi data and model of adsorption–desorption with photocatalytic reaction at 120 and 150 °C desorption temperatures in (a) the airtight chamber and (b) the small box.

The FQE is always less than the quantum yield, because it incorporates all incident light. The FQE is calculated for the data of Shiraishi et al. by making two estimations: (1) The reaction rate is first order in CH_2O, and (2) 1 mW/cm^2 corresponds to $\sim 2 \times 10^{15}$ photons/(s cm^2) at a wavelength of 350 nm, as calculated using the Planck relation and the wave theory of light [37]:

$$E = h\nu, \tag{13}$$

$$\lambda\nu = c, \tag{14}$$

and

$$\frac{\#\text{photons}}{\text{cm}^2\ \text{s}} = \frac{E/\text{cm}^2}{h(c/\lambda)}, \tag{15}$$

where E is the total incident photon energy (mW), h is Planck's constant (6.63×10^{-34} J s/photon), c is the speed of light in a vacuum (2.998×10^8 m/s), and λ is the wavelength (in nm). We calculate the maximum FQEs for the Shiraishi et al. reaction data as 6×10^{-4} at 180 °C, and 2×10^{-3} molecules/photon at desorption temperatures of 120 and 150 °C. A comparison of our FQEs for the data of Shiraishi et al. with other literature is given in Table 1. Our calculated FQEs for the data of Shiraishi et al. are lower than those of other authors.

The model developed here for the combined rotating adsorbent–PCO reactor system developed by Shiraishi et al. [29] provides a technique for evaluating the adsorption, desorption, and reaction rate constants, as well as the adsorption equilibrium constants. This engineering kinetic model can be broadly applied to design-related systems with different adsorption/desorption temperatures, adsorbent materials, and room (chamber) sizes.

4. Conclusion

A reaction engineering model has been developed for the novel combination of a rotating honeycomb adsorbent with a photocatalytic reactor. The model assumes that the adsorption, desorption, and reaction steps are first order with respect to CH_2O. All model parameters were evaluated from the batch data of Shiraishi et al. [29]. Two models were developed: adsorption–desorption-only and adsorption–desorption with PCO reaction. Both models qualitatively describe the observed behavior of gas-phase CH_2O concentrations versus time. In the adsorption–desorption-only experiments, the model describes both transient and asymptotic steady-state values in the airtight chamber and the small box. In the adsorption–desorption with reaction experiments, the model again adequately represents the data. The pseudo-first-order reaction rate constants determined through model fitting fall in the same range as that derived in five literature studies.

Acknowledgments

The authors acknowledge support from the State of North Carolina for funding this research. The authors also thank the Park Foundation Scholarship at North Carolina State University for funding the work of Lao Yang

Appendix A. Nomenclature

δ	formal quantum efficiency (FQE)
Φ_{overall}	quantum yield
h	Planck's constant (6.63×10^{-34} J s/photon)
λ	wavelength (nm)
c	speed of light in vacuum (2.998×10^8 m/s)
C_0	initial CH_2O concentration in the airtight chamber (mg/cm^3)
C_{AC}	CH_2O concentration in the airtight chamber (mg/cm^3)
C_{CHR}	CH_2O concentration on the ceramic honeycomb rotor (mg/cm^3)
C_{SB}	CH_2O concentration in the small box (mg/cm^3)
E	photon specific energy (mW)

$E_{A,des}$ activation energy for the CH_2O desorption rate constant between the ceramic honeycomb rotor and the small box (J/mol)

$k_{ads}(T_{ads})$ CH_2O adsorption rate constant between the ceramic honeycomb rotor and the airtight chamber (s^{-1})

$k_{ads}(T_{des})$ CH_2O adsorption rate constant between the ceramic honeycomb rotor and the small box (s^{-1})

$k_{cat}(T_{des})$ CH_2O pseudo-first-order kinetic rate constant in the photocatalytic reactor (s^{-1})

$k_{des}(T_{ads})$ CH_2O desorption rate constant between the ceramic honeycomb rotor and the airtight chamber (s^{-1})

$k_{des}(T_{des})$ CH_2O desorption rate constant on the ceramic honeycomb rotor in the small box (s^{-1})

$k_{des,0}$ pre-exponential factor for the CH_2O desorption rate constant between the ceramic honeycomb rotor and the small box

$K_{AC\text{-}CHR}(T_{ads})$ CH_2O adsorption equilibrium constant between the airtight chamber and the ceramic honeycomb rotor

$K_{SB\text{-}CHR}(T_{des})$ CH_2O adsorption equilibrium constant between the small box and the ceramic honeycomb rotor

r_{ads} rate of CH_2O adsorption on the ceramic honeycomb rotor from the airtight chamber ($mg/(m^3\,s)$)

r_{cat} rate of CH_2O photocatalyzed oxidation by TiO_2 ($mg/(m^3\,s)$)

r_{des} rate of CH_2O desorption on the ceramic honeycomb rotor to the small box ($mg/(m^3\,s)$)

t time (s)

R Universal gas constant (8.314 J/(mol K))

V_{AC} volume of the airtight chamber (10 m^3)

V_{CHR} volume of the ceramic honeycomb rotor

V_{rxr} volume of the photocatalytic reactor ($\sim$0.014 m^3)

V_{SB} Volume of the small box (0.09 m^3)

References

[1] Indoor Air Quality Information Clearinghouse, Sick Building Syndrome, U.S. Environmental Protection Agency, 1991.

[2] R.M. Heck, R.J. Farrauto, S.T. Gulati, Catalytic Air Pollution Control Commercial Technology, second ed., Wiley, New York, NY, 2002, p. 391.

[3] U.S. Environmental Protection Agency, Code of Federal Regulations, title 40, chap. 1, subchapter C, §51.100(s), 2005.

[4] Occupational Safety and Health Administration, OSHA Technical Manual, section III, chap. 2, U.S. Department of Labor, 2005.

[5] U.S. Consumer Product Safety Commission, An Update on Formaldehyde, 1997.

[6] D.T. Allen, D.R. Shonnard, Green Engineering: Environmentally Conscious Design of Chemical Processes, Prentice Hall, Upper Saddle River, NJ, 2002, p. 552.

[7] H.E. Hesketh, F.L. Cross, Odor Control Including Hazardous/Toxic Odors, Technomic Publishing Company, Lancaster, PA, 1989 p. 86.

[8] S. Aguado, A.C. Polo, M.P. Bernal, J. Coronas, J. Santamaria, J. Membr. Sci. 240 (2004) 159.

[9] A.C. Stern, Air Pollution: Sources of Air Pollution and Their Control, vol. 3, second ed., Academic Press, New York, NY, 1968, p. 866.

[10] J. Peral, D.F. Ollis, J. Catal. 136 (1992) 554.

[11] T.N. Obee, R.T. Brown, Environ. Sci. Technol. 29 (1995) 1223.

[12] T.N. Obee, Environ. Sci. Technol. 30 (1996) 3578.

[13] Y.P. Zhang, R. Yang, R.Y. Zhao, Atmos. Environ. 37 (2003) 3395.

[14] L. Saadoun, J.A. Ayllon, J. Jimenez-Becerril, J. Peral, X. Domenech, R. Rodriguez-Clemente, Mater. Res. Bull. 35 (2000) 193.

[15] T. Noguchi, A. Fujishima, P. Sawunyama, H. Kazuhito, Environ. Sci. Technol. 32 (1998) 3831.

[16] W.H. Ching, M. Leung, D.Y.C. Leung, Sol. Energy 77 (2004) 129.

[17] C.H. Ao, S.C. Lee, J.Z. Yu, J.H. Xu, Appl. Catal. B: Environ. 54 (2004) 41.

[18] M.R. Nimlos, E.J. Wolfrum, M.L. Brewer, J.A. Fennell, G. Bintner, Environ. Sci. Technol. 30 (1996) 3102.

[19] A.C. Lukaski, D.S. Muggli, J. Catal. 223 (2004) 250.

[20] D.S. Muggli, J.T. McCue, J.L. Falconer, J. Catal. 173 (1998) 470.

[21] C.C. Chuang, W.C. Wu, M.C. Huang, I.C. Huang, J.L. Lin, J. Catal. 185 (1999) 423.

[22] M.L. Sauer, D.F. Ollis, J. Catal. 158 (1996) 570.

[23] K. Suzuki, in: D.F. Ollis, H. Al-Ekabi (Eds.), Photocatalytic Air Purification on TiO_2 Coated Honeycomb Support, 1st International Conference on TiO_2 Photocatalytic Purification and Treatment of Water and Air, London, Ontario, Canada, Elsevier Science Publishers B.V., Amsterdam, 1992, p. 820.

[24] M.L. Sauer, D.F. Ollis, J. Catal. 149 (1994) 81.

[25] G.S. Son, S.W. Yun, S.H. Ko, J.W. Song, K.Y. Lee, J. Adv. Oxid. Technol. 6 (2003) 80.

[26] F.T. Chang, Y.C. Lin, H.L. Bai, B.S. Pei, J. Air Waste Manage. Assoc. 53 (2003) 1384.

[27] Y. Mitsuma, Y. Ota, T. Hirose, J. Chem. Eng. Jpn. 31 (1998) 482.

[28] C.H. Ao, S.C. Lee, Chem. Eng. Sci. 60 (2005) 103.

[29] F. Shiraishi, S. Yamaguchi, Y. Ohbuchi, Chem. Eng. Sci. 58 (2003) 929.

[30] M. Lewandowski, D.F. Ollis, Appl. Catal. B: Environ. 43 (2003) 309.

[31] J.M. Thomas, W.J. Thomas, Principles and Practice of Heterogeneous Catalysis, VCH, New York, NY, 1997, p. 669.

[32] S.A. Larson, J.L. Falconer, Catal. Lett. 44 (1997) 57.

[33] R.J. Farrauto, C.H. Bartholomew, Fundamentals of Industrial Catalytic Processes, first ed., Blackie Academic & Professional, London, UK, 1997, p. 754.

[34] H. Okabe, Photochemistry of Small Molecules, Wiley, New York, NY, 1978, p. 431.

[35] A. Mills, S. LeHunte, J. Photochem. Photobiol. A: Chem. 108 (1997) 1.

[36] A. Mills, A. Lepre, N. Elliott, S. Bhopal, I.P. Parkin, S.A. O'Neill, J. Photochem. Photobiol. A: Chem. 160 (2003) 213.

[37] N. Serpone, E. Pelizzetti, Photocatalysis: Fundamentals and Applications, Wiley, New York, NY, 1989, p. 650.